Liprin-α controls stress fiber formation by binding to mDia and regulating its membrane localization

Satoko Sakamoto[1], Toshimasa Ishizaki[1], Katsuya Okawa[2], Sadanori Watanabe[1], Takatoshi Arakawa[3], Naoki Watanabe[1,*] and Shuh Narumiya[1,‡]

[1]Department of Pharmacology, Kyoto University Graduate School of Medicine, Kyoto 606-8501, Japan
[2]Drug Discovery Research Laboratories, Kyowa Hakko Kirin, Shizuoka 411-8731, Japan
[3]Department of Cell Biology, Kyoto University Graduate School of Medicine, Kyoto 606-8501, Japan

*Present address: Laboratory of Single-Molecule Cell Biology, Tohoku University Graduate School of Life Sciences, Sendai 980-8578, Japan
‡Author for correspondence (snaru@mfour.med.kyoto-u.ac.jp)

Accepted 11 July 2011
Journal of Cell Science 125, 108–120

doi: 10.1242/jcs.087411

Summary

Regulation of the actin cytoskeleton is crucial for cell morphology and migration. mDia is an actin nucleator that produces unbranched actin filaments downstream of Rho. However, the mechanisms by which mDia activity is regulated in the cell remain unknown. We pulled down Liprin-α as an mDia-binding protein. The binding is mediated through the central region of Liprin-α and through the N-terminal Dia-inhibitory domain (DID) and dimerization domain (DD) of mDia. Liprin-α competes with Dia autoregulatory domain (DAD) for binding to DID, and binds preferably to the open form of mDia. Overexpression of a Liprin-α fragment containing the mDia-binding region decreases localization of mDia to the plasma membrane and attenuates the Rho–mDia-mediated formation of stress fibers in cultured cells. Conversely, depletion of Liprin-α by RNA interference (RNAi) increases the amount of mDia in the membrane fraction and enhances formation of actin stress fibers. Thus, Liprin-α negatively regulates the activity of mDia in the cell by displacing it from the plasma membrane through binding to the DID-DD region.

Key words: Actin cytoskeleton, mDia, Rho, Liprin-α

Introduction

Temporal and spatial remodeling of the actin cytoskeleton plays a central role in cell morphology, polarity, migration and cytokinesis. One of the key molecules that regulate actin remodeling is the small GTPase Rho. Rho shuttles between the inactive GDP-bound form and the active GTP-bound form, and works as a molecular switch in actin remodeling in response to both extra- and intracellular stimuli (Hall, 2005). Mammalian homolog of Diaphanous (mDia), a group of formins, is one of the Rho effectors, and is involved in the Rho-mediated assembly of actin stress fibers (Watanabe et al., 1999; Hotulainen and Lappalainen, 2006), the formation of the contractile ring (Watanabe et al., 2008), and formation of filopodia (Schirenbeck et al., 2005). Formins comprise a large family that is conserved from yeast to mammals. More than 30 formins have been described to date, with more than 15 members in vertebrates (Higgs, 2005). Formins are characterized by the presence of the highly conserved formin homology (FH) 1 and 2 domains and produce unbranched, long actin filaments. The FH2 domain catalyzes de novo actin nucleation and polymerization, being persistently associated with the barbed end of nascent filaments and protecting them from capping proteins (Moseley et al., 2004; Higgs, 2005; Chesarone et al., 2010). The adjacent FH1 domain recruits profilin–actin complexes and accelerates filament elongation. In addition to these domains, mDia contains GTPase-binding domain (GBD), Dia-inhibitory domain (DID), dimerization domain (DD) and coiled-coil (CC) domain in the N-terminus, and Dia autoregulatory domain (DAD) in the C-terminus (Chesarone et al., 2010). mDia is auto-inhibited via an intramolecular interaction between DID and DAD, which inhibits the ability of FH1-FH2 to nucleate and elongate actin filaments in vitro and in vivo. Binding of GTP-bound Rho to GBD disrupts this intramolecular interaction and leads to activation of mDia (Watanabe et al., 1999). Activated mDia then induces actin polymerization through the FH1-FH2 domain. Intriguingly, whereas purified formins remain bound to and elongate the barbed end for many minutes to produce long filaments (Pruyne et al., 2002; Sagot et al., 2002; Higashida et al., 2004), actin cables and the cytokinetic ring assembled by yeast formins in vivo are comprised of relatively short filaments of 0.3–2.3 μm in length (Kamasaki et al., 2005; Kamasaki et al., 2007). These findings indicate that the ability of mDia is crucially regulated in the cell. Notably, release of auto-inhibition by activated Rho is suggested to induce not only actin polymerizing activity but also membrane localization of mDia in the cell (Chesarone et al., 2010). Because endogenous mDia1, although sometimes enriched at the extended edge of cells, is mainly distributed diffusely in the cytoplasm (Watanabe et al. 1997; Brandt et al., 2007), membrane targeting of mDia molecules has been studied using truncation fragments. Such studies have revealed that the membrane localization of mDia is mediated through its DID-DD-CC domains in addition to its binding to Rho (Seth et al., 2006; Brandt et al., 2007; Watanabe et al., 2010; Gorelik et al., 2011). These results suggest that, in addition to regulation by Rho, the activity and localization of mDia are regulated by its interaction with DID-binding proteins. This possibility is also suggested by the fact that N-terminally truncated mutants of mDia lacking DID, such as mDia1ΔN3, expressed in the cell produce longer

Journal of Cell Science

filaments than does full-length mDia1 (Higashida et al., 2004; Higashida et al., 2008). To search for such DID-binding proteins, we carried out a pull-down assay with an N-terminal mDia1 fragment as the bait. We have identified Liprin-α as an mDia-interacting protein, and found that this protein regulates the membrane localization of mDia through direct binding to the DID-DD region, and modulates the amount of actin filaments in the cell.

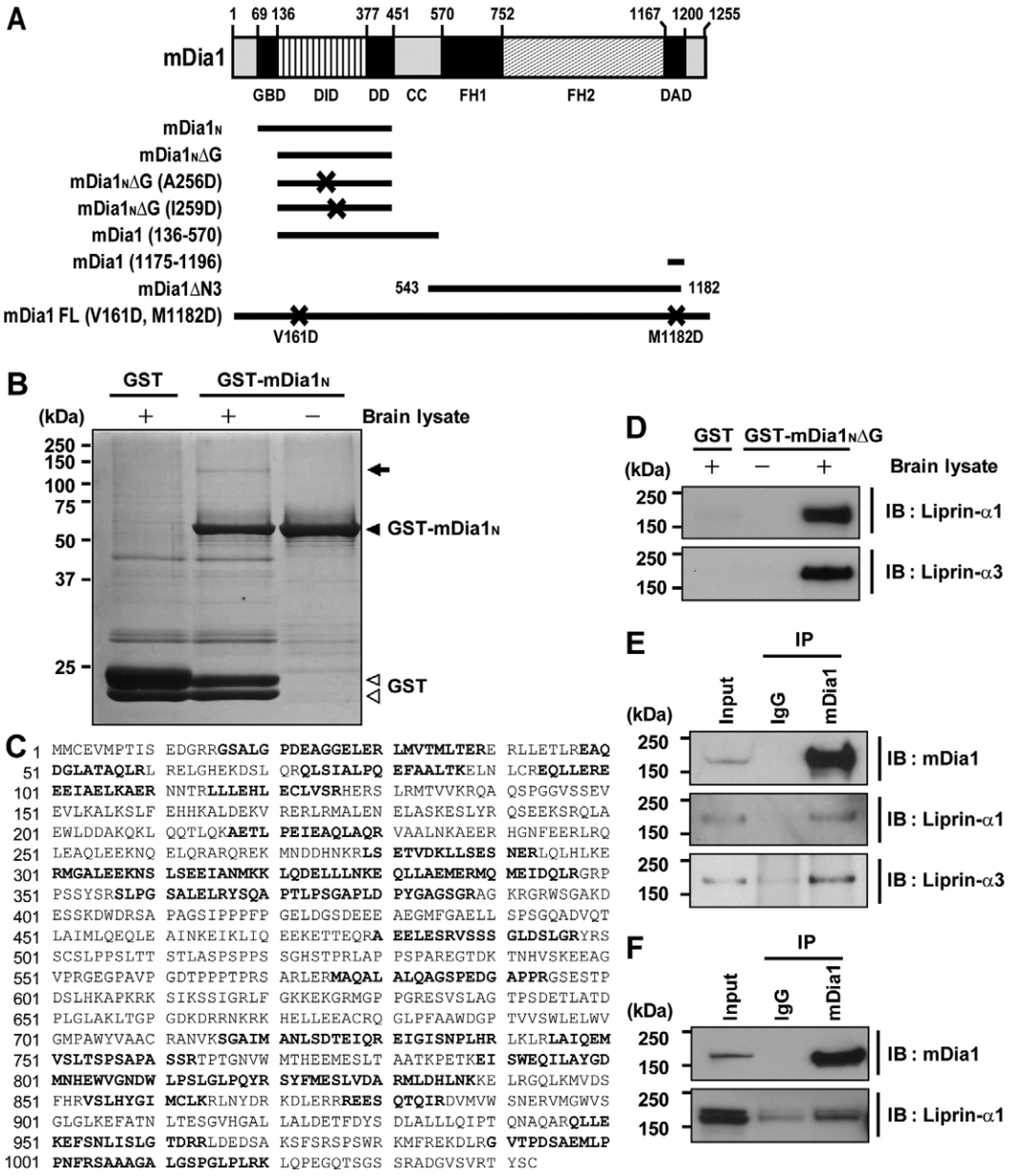

Fig. 1. Identification of Liprin-α as an mDia binding protein. (**A**) Domain structure of mDia1 and truncation mutants. Amino acid numbers for the N- and C-terminal residues of each domain and mutant protein are shown. X indicates the position of mutation. (**B**) Pull-down experiment. GST–mDia1$_N$ or GST was incubated with mouse brain lysates (+) or an equal volume of the lysis buffer (–), precipitated with GSH Sepharose, and subjected to SDS-PAGE. CBB staining of the gel is shown. An arrow indicates an mDia-interacting protein of 160 kDa. Black and white arrowheads indicate GST–mDia1$_N$ and GST, respectively. (**C**) Identification of the mDia-interacting protein as Liprin-α3. The amino acid sequence of Liprin-α3 (GenBank accession number AAH58404) is shown. Eighteen peptides of the mDia1-interacting protein identified by mass spectrometric analysis are highlighted in bold letters. (**D**) Interaction of Liprin-α1 and Liprin-α3 with mDia1$_N$ΔG. The mouse brain lysates were subjected to the pull-down experiment as described for B, with mDia1$_N$ΔG as a bait. The precipitates obtained were used for SDS-PAGE and probed with antibodies to Liprin-α1 or Liprin-α3. (**E**) Co-immunoprecipitation of Liprin-α1 and Liprin-α3 with mDia1 from mouse brain lysates. Mouse brain RIPA lysates were incubated with anti-mDia1 antibody or control rabbit IgG. The immune complex was precipitated with Protein-G–Sepharose, and analyzed by immunoblotting with antibodies to mDia1 (upper panel), Liprin-α1 (middle panel) and Liprin-α3 (bottom panel). Input was 15 μl out of 4 ml of the total extract, and 62.5 μl equivalent of the total extract was used as the immunoprecipitates. (**F**) Co-immunoprecipitation of Liprin-α1 with mDia1 from 293F cell lysates. 293F cell lysates were incubated with anti-mDia1 antibody or control rabbit IgG. The immune complex was precipitated with Protein-G–Sepharose, and analyzed by immunoblotting with antibodies against mDia1 (upper panel) and Liprin-α1 (bottom panel). Input applied was 18.75 μl out of 3 ml of the total lysates, and 62.5 μl equivalent of the total lysates was used in the immunoprecipitates.

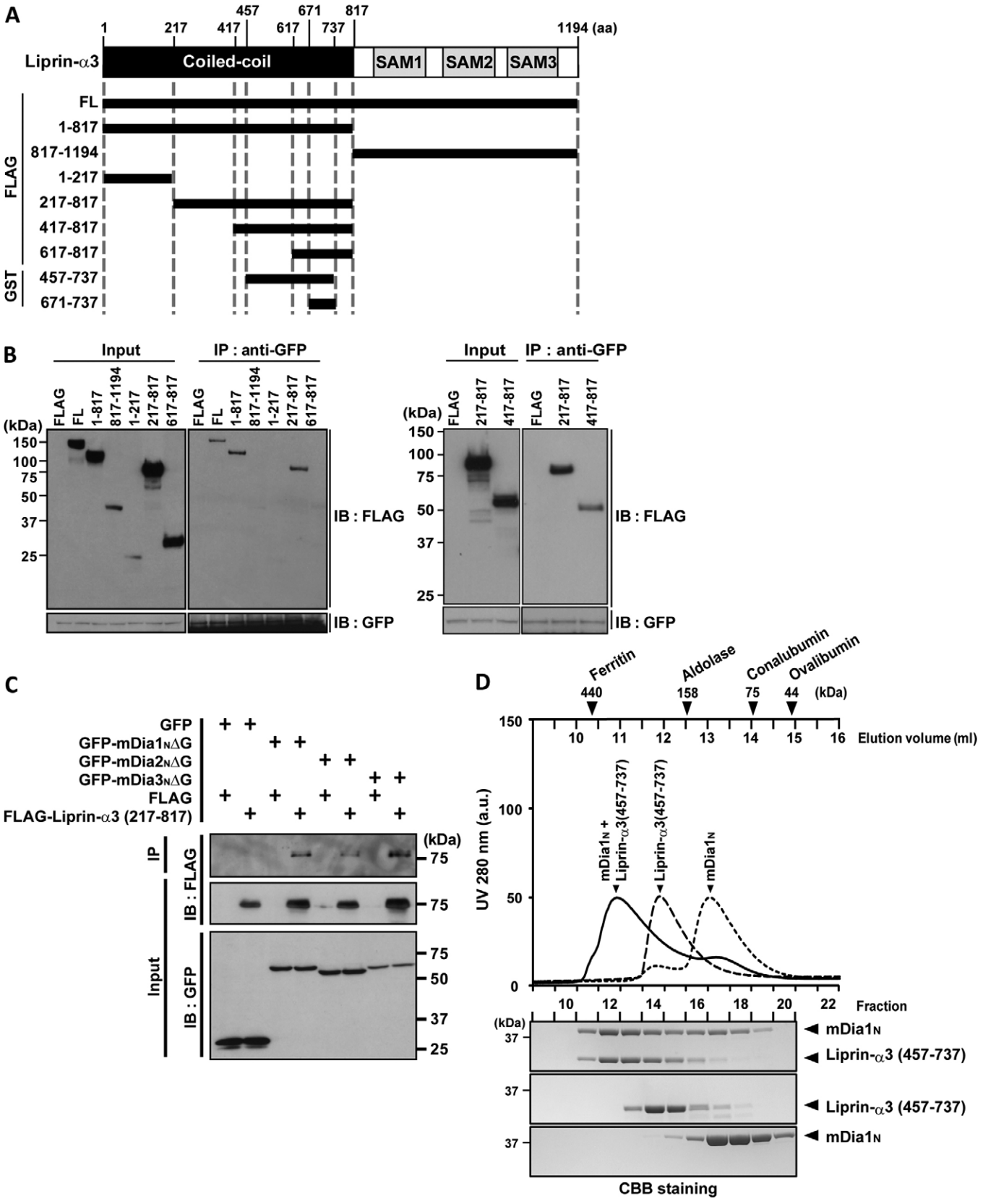

Fig. 2. See next page for legend.

Results

Identification of Liprin-α as an mDia-binding protein

To identify proteins that interact with mDia1, we used a glutathione S-transferase (GST) fusion of an N-terminal GBD-DID-DD fragment of mDia1, amino acids 69–451 (mDia1$_N$) (Rose et al., 2005), as bait, and performed a pull-down assay (Fig. 1A). This procedure specifically pulled down a 160 kDa protein from the S100 fraction of the mouse brain (Fig. 1B). This protein retained the interaction with up to 200 mM NaCl washing (data not shown). Mass spectrometry of digests of the protein identified 18 peptides that are all present in Liprin-α3 (Fig. 1C). Liprin-α is a protein enriched in synaptic structures, and consists of isoforms 1–4 in mammals (Serra-Pages et al., 1995; Serra-Pages et al., 1998; Spangler and Hoogenraad, 2007). Immunoblot analysis, using antibodies to Liprin-α1 and Liprin-α3, revealed that GST–mDia1$_N$ pulled down not only Liprin-α3 but also Liprin-α1 (supplementary material Fig. S1A) from the brain S100 fraction. Furthermore, mDia1$_N$ΔG, an N-terminal fragment containing DID-DD without GBD, also interacted with both Liprin-α isoforms (Fig. 1D), suggesting that GBD is dispensable for binding to Liprin-α. An antibody to mDia1 (Watanabe et al., 1997) co-immunoprecipitated endogenous Liprin-α isoforms from mouse brain lysate (Fig. 1E) and 293F cell lysate (Fig. 1F), verifying endogenous interaction of the two proteins.

mDia directly binds to Liprin-α3 through its central region

Liprin-α isoforms consist of an approximately 800 amino acid-long coiled-coil domain in the N-terminus, followed by three consecutive sterile alpha motif (SAM) domains in the C-terminus (Spangler and Hoogenraad, 2007). To characterize the domain in Liprin-α that interacts with mDia1, a series of FLAG-tagged deletion mutants of Liprin-α3 (Fig. 2A) were expressed with GFP–mDia1$_N$ΔG in HeLa cells, and subjected to immunoprecipitation. In this assay, GFP–mDia1$_N$ΔG co-precipitated FLAG-tagged full-length (FL) Liprin-α3 (Fig. 2B), and, conversely, FLAG–Liprin-α3(FL) co-precipitated GFP–mDia1$_N$ΔG (supplementary material Fig. S1B). Under these conditions, GFP–mDia1$_N$ΔG co-precipitated the Liprin-α3 fragments of amino acids 1–817, 217–817 and 417–817 but not those of amino acids 817–1194 (Fig. 2B). No precipitation was found with the fragments of amino acids 1–217 or 617–817 (Fig. 2B). GFP alone did not precipitate any Liprin-α3 proteins (supplementary material Fig. S1C). We then expressed the N-terminal domain of mDia2 or mDia3 with FLAG–Liprin-α3(217–817), and examined the interaction. Liprin-α3(217–817) also precipitated GFP–mDia2$_N$ΔG and GFP–mDia3$_N$ΔG (Fig. 2C). These results indicate that all three mDia isoforms interact with Liprin-α3 through their DID-DD regions.

To examine whether mDia1 and Liprin-α3 directly interact, we prepared recombinant mDia1$_N$ and Liprin-α3(417–817). However, the latter protein underwent proteolytic degradation during preparation and so we chopped it to Liprin-α3(457–737), which was prepared as a single band protein on SDS-PAGE. Using these proteins, we first performed analytical gel filtration. We prepared mDia1$_N$ (44 kDa) and Liprin-α3(457–737) (30 kDa) proteins separately, and incubated 150 μg of Liprin-α3(457–737) with 150 μg of mDia1$_N$ for 30 minutes at 4℃. We then applied either this incubation mixture or 150 μg each of either protein to a Sephadex G200 column for gel filtration. Whereas Liprin-α3(457–737) or mDia1$_N$ applied alone were eluted in a single peak at the elution volume of 12 ml (estimated relative molecular mass, Mr, 195 kDa) or 13 ml (estimated Mr 130 kDa), respectively, the incubation mixture of these proteins yielded a new protein peak at the elution volume of 11 ml (estimated Mr 300 kDa) as well as the aforementioned two peaks (Fig. 2D). Coomassie Brilliant Blue (CBB) staining of the fractions detected Liprin-α3(457–737) and mDia1$_N$, with a protein ratio of 1:1 in the peak fractions of the mixture (Fig. 2D). Given the estimated Mr, these results indicate that mDia1$_N$ and Liprin-α3(457–737) made a tetramer–tetramer complex. We next used surface plasmon resonance to measure the binding affinity between GST–Liprin-α3 and mDia1$_N$. Because Liprin-α3(457–737) adhered to the sensor tip, we prepared Liprin-α3(671–737) to use instead. Although a larger protein including this sequence, Liprin-α3(617–817), did not precipitate with mDia1$_N$ΔG in the coexpression experiment (Fig. 2B), Liprin-α3(671–737) interacted weakly with mDia1$_N$ on BIAcore. The association (k_a) and dissociation (k_d) rate constants and the equilibrium dissociation constant (K_D) of binding of GST–Liprin-α3(671–737) and mDia1$_N$ were 2.04×10^4 $M^{-1}second^{-1}$, 0.021 $second^{-1}$ and 1.03×10^{-6} M, respectively.

Liprin-α preferably binds to the open form of mDia

To further confirm direct binding of mDia1 and Liprin-α3, we incubated GST–mDia1$_N$ΔG or GST and Liprin-α3(457–737) in vitro, and precipitated GST proteins with glutathione (GSH) Sepharose. GST–mDia1$_N$ΔG specifically pulled down Liprin-α3(457–737) (Fig. 3A). The Liprin-α-binding domain of mDia1 defined above contains DID, which serves as a binding site for DAD. A256D (alanine 256 changed to aspartic acid) and I259D (isoleucine 259 to aspartic acid) mutations in DID affects its binding to DAD in vitro (Lammers et al., 2005). We therefore examined the effect of these DID mutations on Liprin-α3(457–737) binding. Whereas wild-type mDia1$_N$ΔG effectively pulled down Liprin-α3(457–737), the mDia1$_N$ΔG(A256D) and mDia1$_N$ΔG(I259D) precipitated markedly less amounts of Liprin-α3(457–737) (Fig. 3A). These results indicate that alanine 256 and isoleucine 259 are important in binding of mDia1, not

Fig. 2. Liprin-α directly binds to mDia through its central region. (**A**) Representation of Liprin-α3 and truncation mutants. All constructs were tagged with FLAG epitope at the N-terminus except for 457–737 and 671–737 that were tagged with GST and used in gel filtration after GST cleavage and BIAcore, respectively. Amino acid numbers for the N- and C-terminal residues of each mutant protein are shown. (**B**) Identification of the mDia-binding domain in Liprin-α3. GFP–mDia1$_N$ΔG was expressed in HeLa cells together with each of the indicated FLAG–Liprin-α3 proteins. The cell lysates were subjected to immunoprecipitation with anti-GFP antibody. The immunoprecipitates (IP, right panels) as well as lysates (Input, left panels) were analyzed by immunoblotting (IB) with anti-GFP antibody and anti-FLAG antibody. (**C**) Interaction of all three mDia isoforms with Liprin-α. GFP–mDia1$_N$ΔG, GFP–mDia2$_N$ΔG or GFP–mDia3$_N$ΔG were expressed with FLAG–Liprin-α3(217–817) in HeLa cells, and immunoprecipitation was performed as described for B. (**D**) Analytical gel filtration. Recombinant proteins of Liprin-α3(457–737) and mDia1$_N$ were prepared and either used separately or incubated in equal amounts. mDia1$_N$ alone (dashed line), Liprin-α3(457–737) alone (broken line) or the incubation mixture (solid line) was loaded on a Superdex G200 10/30 column and protein elution was monitored by measuring absorbance at 280 nm (upper panel). The column was calibrated with ferritin, aldolase, conalubumin and ovalubumin. Lower panels show CBB staining of indicated fractions for indicated proteins.

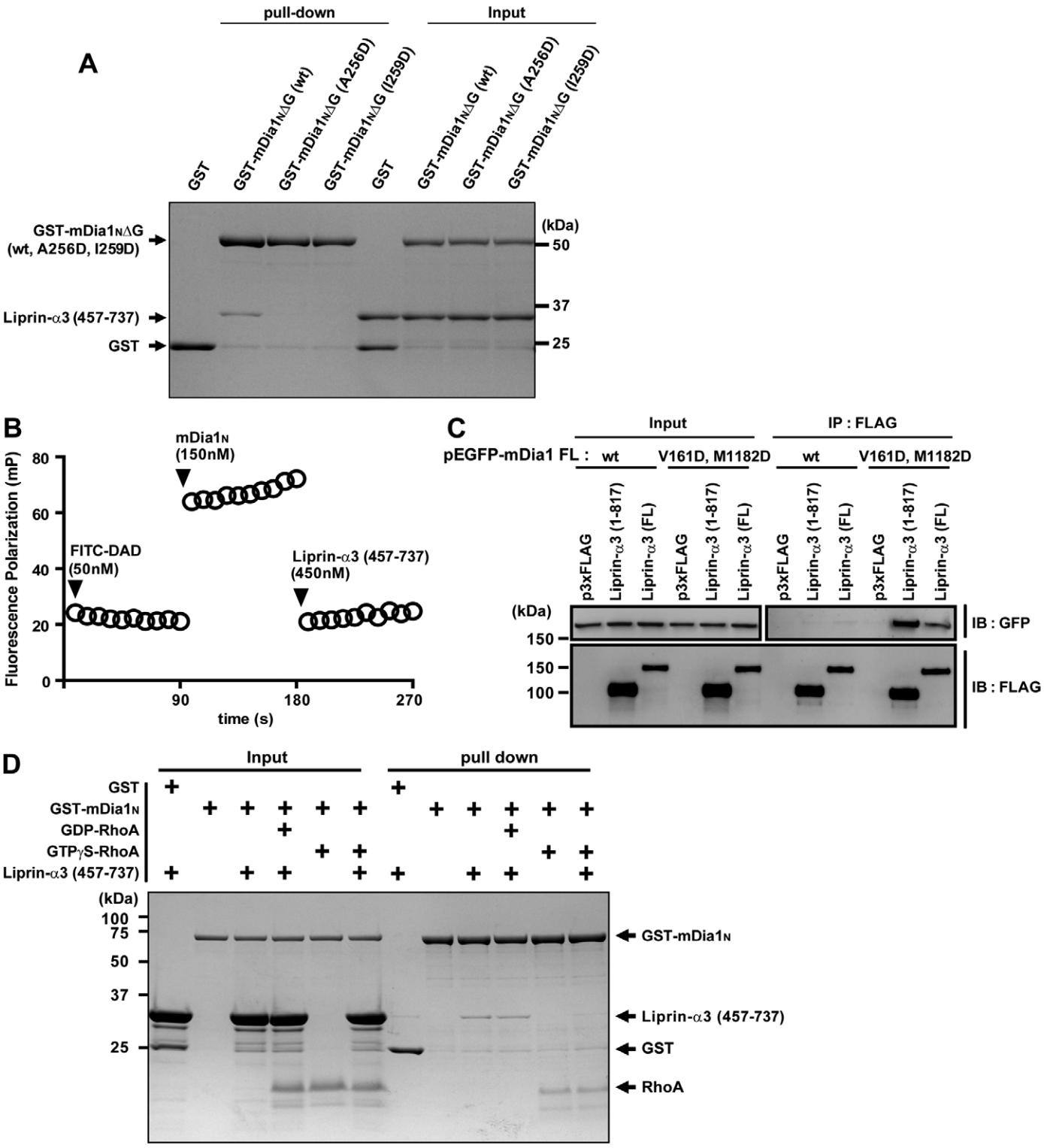

Fig. 3. Liprin-α preferably binds to the open form of mDia. (**A**) A256D and I259D mutations impair binding of mDia1$_N$ΔG to Liprin-α3. Liprin-α3(457–737) was incubated with either GST or GST–mDia1$_N$ΔG, GST–mDia1$_N$ΔG(A256D) or GST–mDia1$_N$ΔG(I259D) conjugated to GSH Sepharose beads. Co-precipitated proteins were analyzed by SDS-PAGE and CBB staining. (**B**) Fluorescence polarization assay. FITC-labeled mDia1-DAD peptide(1175–1196) was mixed with indicated concentrations of recombinant mDia1$_N$ and then with Liprin-α3(457–737) and the fluorescence polarization was measured. (**C**) Liprin-α3 binds to an open form of mDia1. GFP–mDia1(FL) or GFP–mDia1(FL)(V161D, M1182D) was expressed in HeLa cells with FLAG–Liprin-α3(1–817), FLAG–Liprin-α3(FL) or FLAG. Immunoprecipitation was performed with FLAG affinity gel. Immunoprecipitates (IP, right panels) as well as lysates (Input, left panels) were analyzed by immunoblotting (IB) with anti-GFP and anti-FLAG antibodies. (**D**) Impaired binding of Liprin-α3 to mDia1$_N$ in complex with GTPγS–RhoA. GST or GST–mDia1$_N$ conjugated to GSH Sepharose beads were pre-incubated with GDP–RhoA or GTPγS–RhoA, followed by incubation with Liprin-α3(457–737), and precipitated. Bound proteins were analyzed by SDS-PAGE, followed by CBB staining.

only to DAD but also to Liprin-α, and suggest that binding sites in DID of mDia1 for DAD and Liprin-α3 might overlap. To test this, we performed fluorescent polarization assays. Polarization of a fluorescein isothiocyanate (FITC)-labeled 22-mer DAD peptide (amino acids 1175–1196) was strongly increased after addition of a threefold excess of $mDia1_N$ as a result of the decreased mobility of the higher molecular mass DAD–$mDia1_N$ complex, as first described by Rose et al. (Rose et al., 2005). The addition of a ninefold excess of Liprin-α3(457–737) over DAD to this reaction quickly reduced the polarization (Fig. 3B), suggesting that Liprin-α competed with DAD for binding to $mDia1_N$ and released DAD from the $mDia1_N$. We then wondered whether Liprin-α binds to the inactive, closed form of mDia by disrupting the intramolecular interaction between DID and DAD. To test this, we co-transfected HeLa cells with either pEGFP–mDia1(FL) or pEGFP–mDia1(FL)(V161D,M1182D) and either p3 × FLAG–Liprin-α3(1–817) or p3 × FLAG–Liprin-α3(FL), and performed immunoprecipitation using an anti-FLAG antibody. The mutations at valine 161 and methionine 1182 interfere with the Rho binding and the DID–DAD interaction, respectively (Lammers et al., 2005; Otomo et al., 2005). Expression of the V161D, M1182D mutant strongly induced thin stress fibers (Fig. 4B), indicating that this mutant is the active open form of mDia. Both FLAG-tagged Liprin-α3(1–817) and Liprin-α3(FL) effectively precipitated the mDia1 mutant, but wild-type mDia1 to much lesser extent (Fig. 3C). These results suggest that Liprin-α does not effectively bind to the closed form of mDia by displacing DAD from DID, but preferably binds to

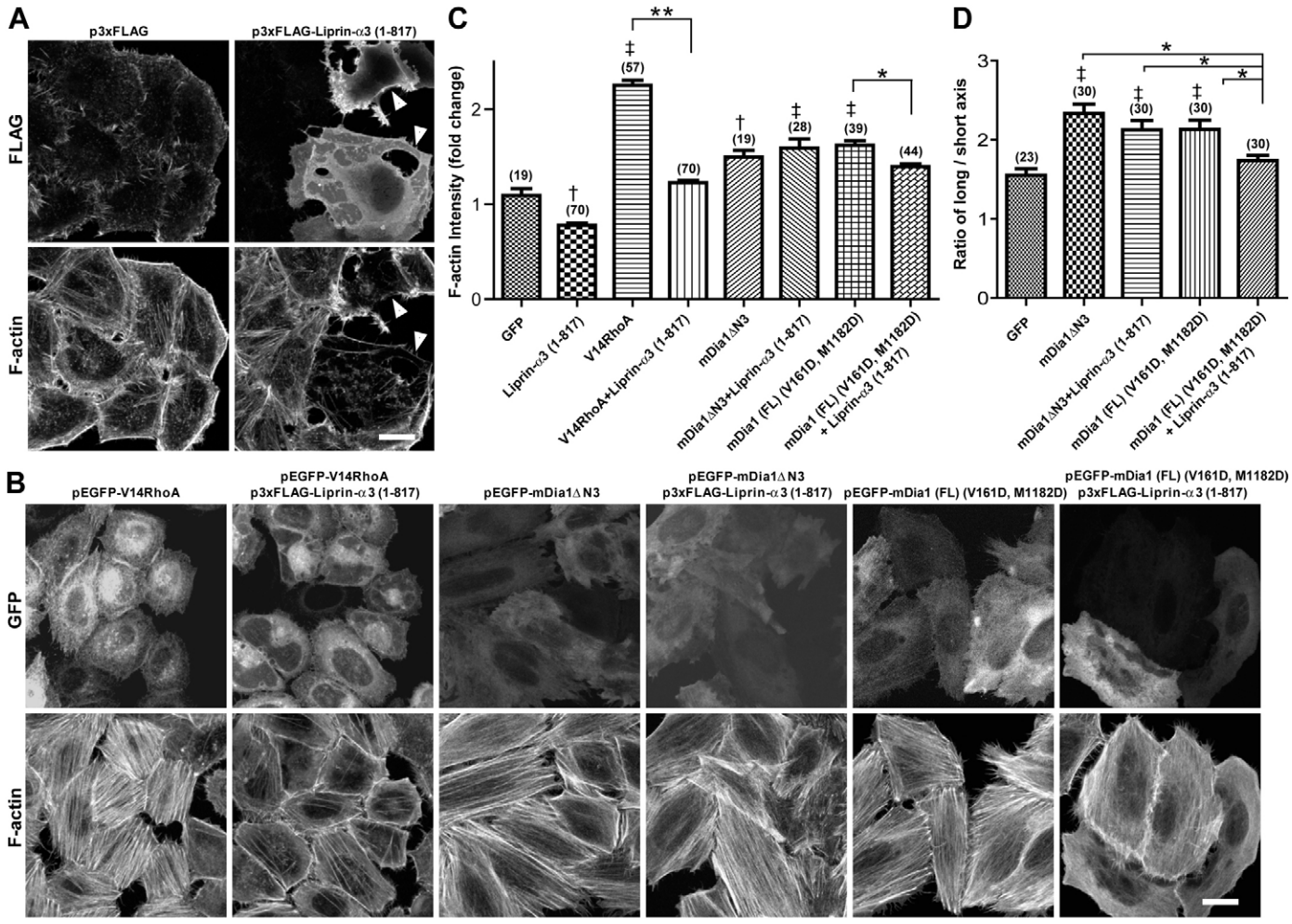

Fig. 4. Overexpression of Liprin-α3(1–817) reduces formation of Rho-induced actin stress fibers in HeLa cells. (**A**) Reduction in formation of actin stress fibers by overexpression of Liprin-α3(1–817) in HeLa cells. HeLa cells were transfected with either p3 × FLAG or p3 × FLAG–Liprin-α3(1–817), fixed and stained with anti-FLAG antibody (upper panels) and Texas-Red–phalloidin (lower panels). Arrowheads indicate cells expressing FLAG–Liprin-α3(1–817). (**B**) Reduction of Rho–mDia-induced stress fibers by overexpression of Liprin-α3(1–817) in HeLa cells. HeLa cells were transfected with indicated plasmids with or without p3 × FLAG–Liprin-α3(1–817), fixed and stained with anti-FLAG antibody (supplementary material Fig. S2D) and Alexa-Fluor-647-labeled phalloidin (lower panels). GFP fluorescence is shown in upper panels. (**C**) Effects of Liprin-α3(1–817) expression on F-actin intensity. The fluorescence intensity of phalloidin staining of transfected cells in each experiment in B was quantitatively compared by normalizing it to that of non-transfected cells in the same experiment (see Materials and Methods). Each column shows the mean + s.e.m. of the number of cells indicated above the column. The results are representative of at least three independent experiments. (**D**) Effects of Liprin-α3(1–817) expression on the long/short axis ratio of cells. HeLa cells were transfected with indicated combination of plasmids, and the ratio of the long/short axis was determined using ImageJ software. The number of cells analyzed is indicated above each column. The results are from three independent experiments. *$P<0.05$ and **$P<0.01$ for indicated comparison. $^{\dagger}P<0.05$ and $^{\ddagger}P<0.01$ compared with GFP-expressing cells. Scale bars: 20 μm.

mDia that has been pre-opened by activated Rho. We therefore examined possible formation of a ternary complex of mDia1, Liprin-α and RhoA. GST fusion of $mDia1_N$ bound to GSH Sepharose was incubated with GDP–RhoA or GTPγS–RhoA. After several washes, Liprin-α3(457–737) were added, incubated for 30 minutes and pulled down with the beads. Liprin-α3(457–737) was pulled down with GST–$mDia1_N$ pre-incubated with GDP–RhoA, but not with GST–$mDia1_N$ in complex with GTPγS–RhoA (Fig. 3D). These results suggest that, although Liprin-α preferably binds to the open form of mDia, it does not form a ternary complex with GTP–RhoA and mDia.

Overexpression of Liprin-α3(1–817) reduces formation of Rho-induced stress fibers in HeLa cells

Given that mDia catalyzes actin polymerization (Watanabe and Higashida, 2004), we examined the effect of Liprin-α expression on the actin cytoskeleton in cells. We expressed FLAG-tagged Liprin-α3(1–817) in HeLa cells (Fig. 4A), and compared the actin cytoskeleton of transfected cells with that of untransfected cells by staining with Texas-Red–phalloidin. Expression of Liprin-α3(1–817) decreased formation of stress fibers and peripheral actin filaments, and reduced the number and size of focal adhesions (Fig. 4A; supplementary material Fig. S2A–C). Some cells exhibited spread morphology, often with concave or hollow spaces in their cell body, and underwent apoptosis. Consistent with the decrease in number of stress fibers, significant decrease in the actin fluorescence intensity compared with control cells was observed (Fig. 4C). By contrast, expression of FLAG–Liprin-α3(1–417) lacking the mDia-binding domain had no effect on the actin cytoskeleton (data not shown), indicating that Liprin-α3(1–817) suppressed endogenous actin filament formation through mDia binding. We then examined the effects of expression of this Liprin-α3 fragment on stress fibers induced by a constitutively active RhoA mutant, V14RhoA. We coexpressed Liprin-α3(1–817) with V14RhoA in HeLa cells, and examined their actin cytoskeleton. Expression of V14RhoA induced thick stress fibers in HeLa cells as reported (Ishizaki et al., 1997). Coexpression of Liprin-α3(1–817) markedly decreased formation of stress fibers induced by the RhoA mutant (Fig. 4B). The fluorescence intensity in the cells coexpressing the Liprin-α3 fragment and V14RhoA was significantly reduced compared with that found in the cells transfected with V14RhoA alone (Fig. 4C). We next expressed GFP–mDia1ΔN3 that lacked the N-terminal Liprin-α-binding domain or GFP–mDia1(FL)(V161D, M1182D) (Fig. 1A) with or without FLAG–Liprin-α3(1–817) in HeLa cells, and compared the actin phenotype of these cells. Expression of both mDia1 mutants induced elongation of HeLa cells, where thin stress fibers were aligned along the long axis of the cells (Fig. 4B,D) (Watanabe et al., 1999). Notably, coexpression with FLAG–Liprin-α3(1–817) remarkably reduced the formation of stress fibers induced by GFP–mDia1(FL)(V161D, M1182D) but not that by mDia1ΔN3 (Fig. 4B; supplementary material Fig. S2D). Consistently, expression of Liprin-α3(1–817) significantly decreased the actin fluorescence intensity and attenuated elongation of cells induced by mDia1(FL)(V161D, M1182D), but the increased actin fluorescence intensity and elongation induced by mDia1ΔN3 was not significantly affected by expression of Liprin-α3(1–817) (Fig. 4C,D). These results suggest that suppression of stress fiber formation by Liprin-α3(1–817) depends on its binding to mDia.

Depletion of Liprin-α increases formation of actin fibers in cultured cells

The above results indicate that endogenous Liprin-α negatively regulates the mDia-mediated formation of actin fibers in cells. We examined this issue first in HeLa cells. HeLa cells express both Liprin-α1 and Liprin-α3 (Fig. 5A; supplementary material Fig. S3A). We transfected HeLa cells with short interfering RNAs (siRNA) against Liprin-α1 (either #1 or #2) and Liprin-α3 (either #1 or #2), with four different combinations of these siRNAs, or with scrambled control siRNA. Transfection efficiency of siRNA in these experiments, as determined by Block-iT Red fluorescent Oligo, was almost 100% (data not shown). Treatment with each siRNA for Liprin-α1, Liprin-α3 or their combinations specifically suppressed the expression of respective Liprin-α isoforms to an almost negligible amount at 48 hours, except for siRNA for Liprin-α3(#2) (Fig. 5A). We then stained the cells with Texas-Red–phalloidin and anti-vinculin antibody. The depletion of each Liprin-α isoform did not apparently change the cell shape, but markedly increased the number of stress fibers and increased the number and size of focal adhesions (Fig. 5B; supplementary material Fig. S3B–D). Although some clusters of cells subjected to RNA interference (RNAi) for either Liprin-α1 or Liprin-α3 did not show the enhanced actin phenotype, combined RNAi for Liprin-α1 and Liprin-α3 increased the number of clusters of cells showing the phenotype.

We then examined whether depletion of human mDia1 suppresses the phenotype caused by Liprin-α1 depletion. Depletion of endogenous mDia1 induced a slight loss of stress fibers, and prevented the enhanced formation of actin fibers induced by depletion of Liprin-α1 (Fig. 5B). To quantify the F-actin fluorescence intensity, we compared the F-actin intensity of cells depleted of Liprin-αs with that of non-transfected cells. Quantitative analysis showed that depletion of Liprin-αs enhanced the F-actin intensity, and that this enhancement was abolished by the depletion of mDia1 (Fig. 5C). The cells treated with siRNA for Liprin-α3(#2) did not show significantly enhanced formation of F-actin (Fig. 5C), probably because of its poor depletion efficiency (Fig. 5A). These results suggest that Liprin-α negatively regulates the mDia-mediated formation of actin fibers and that the two isoforms exert this function redundantly in HeLa cells. Enhanced formation of stress fibers by Liprin-α depletion and its attenuation by additional depletion of mDia1 were also observed in NIH 3T3 cells (supplementary material Fig. S4).

Liprin-αs regulate the membrane localization of mDia through binding to the DID-DD region

It is proposed that mDia isoforms are maintained in an inactive state in the cytosol and recruited to the plasma membrane upon activation (Chesarone et al., 2010). To examine membrane translocation of mDia1, we prepared the cytosol and the membrane fractions from HeLa cells at various times after stimulation with 10% fetal calf serum (FCS), and analyzed the amount of endogenous mDia1 in each fraction by immunoblotting. We found that mDia1 was recruited to the membrane fraction upon stimulation (Fig. 6A). We next examined whether Rho mediates mDia1 translocation to the membrane by expressing V14RhoA in HeLa cells. The amount of mDia1 in the membrane fraction was increased in the cells expressing V14RhoA compared with that in control

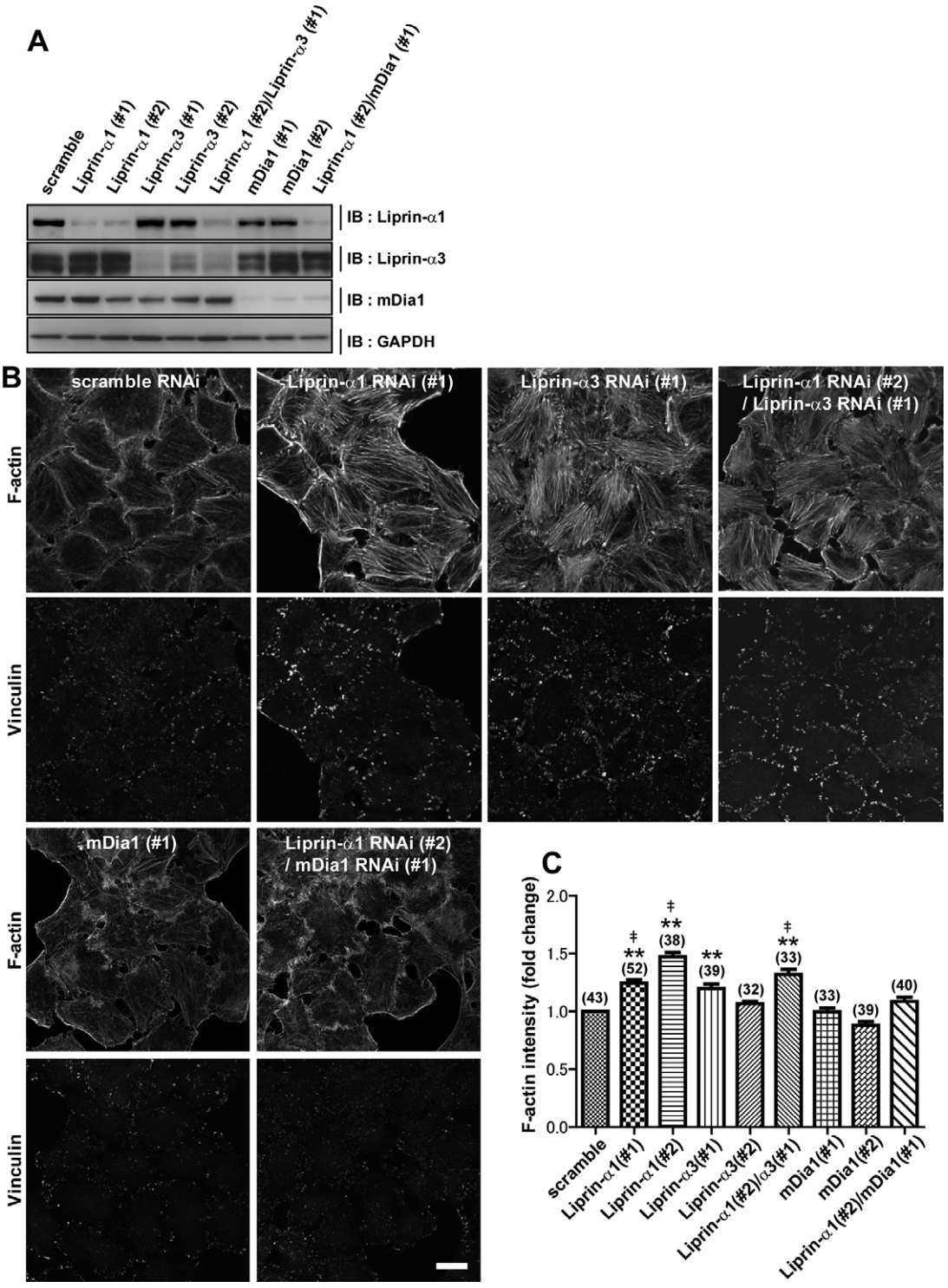

Fig. 5. Depletion of Liprin-α isoforms enhances formation of actin stress fibers in HeLa cells. HeLa cells were transfected with the indicated siRNAs and cultured for 48 hours. (**A**) Depletion of Liprin-α1, Liprin-α3 and mDia1. Cell lysates were prepared and used for immunoblotting with antibodies to Liprin-α1, Liprin-α3, mDia1 and GAPDH. (**B**) Enhancement of formation of mDia1-mediated stress fibers and focal adhesions by depletion of Liprin-α in HeLa cells. The siRNA-transfected cells were fixed and stained with Texas-Red–phalloidin (upper panels) and anti-vinculin antibody (lower panels). Typical results of more than five experiments with siRNA(#1) for Liprin-α1 and siRNA(#1) for Liprin-α3 are shown. Essentially similar results were obtained in experiments with other siRNAs for Liprin-α1 and Liprin-α3 (supplementary material Fig. S3B). Scale bar: 20 μm. (**C**) Effects of Liprin-α depletion on F-actin intensity. Control non-transfected cells were added to siRNA-transfected cells at a ratio of 1:9 at 24 hours after transfection, and cultured together for another 24 hours. The fluorescence intensity of phalloidin staining of transfected cells was normalized to that of non-transfected cells in the same field. The mean + s.e.m. of the normalized values of each group of indicated transfection is shown with the number of cells analyzed indicated above each column. $^{**}P<0.01$ compared with control cells treated with scrambled siRNA. $^{‡}P<0.01$ compared with cells treated with siRNAs for Liprin-α1(#2) and mDia1(#1).

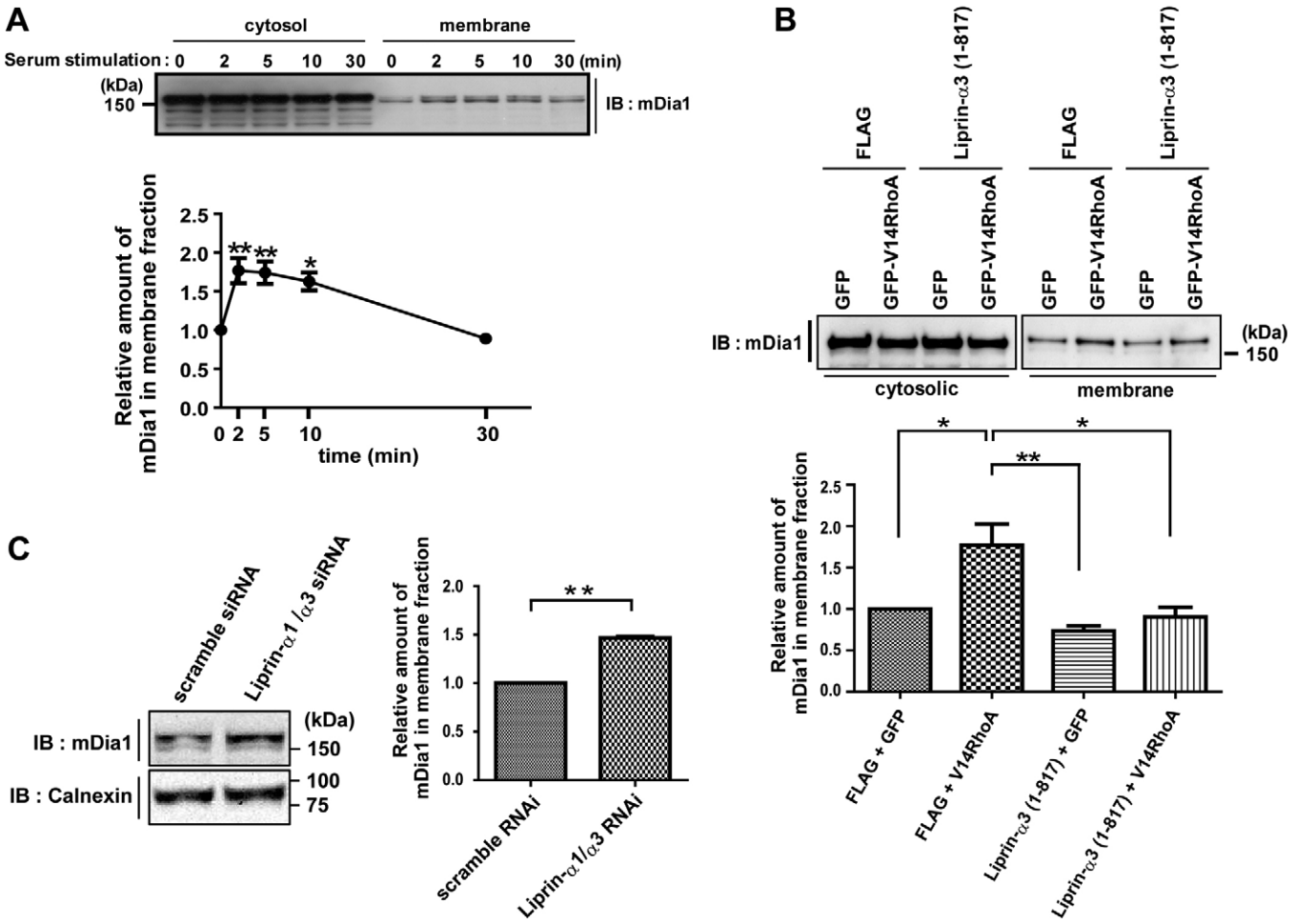

Fig. 6. Liprin-αs regulate enrichment of mDia1 in the membrane fraction. (**A**) Enrichment of mDia1 to the membrane fraction by serum stimulation. Serum-starved HeLa cells were stimulated with 10% FCS. Cytosolic and membrane fractions were prepared at indicated times, and analyzed by immunoblotting using anti-mDia1 antibody. Quantitative measurement of mDia1 in the membrane fraction was performed as described in Materials and Methods and normalized to the band intensity of that at 0 minutes ($n=3$). *$P<0.05$ and **$P<0.01$ compared with control. (**B**) Augmented enrichment of mDia1 to the membrane fraction by expression of active RhoA, and its suppression by coexpression of Liprin-α3(1–817). HeLa cells were transfected with indicated plasmids. After 3 hours, the medium was changed to Opti-MEM, and the cells were cultured for 15 hours. Cytosolic and membrane fractions were collected and then analyzed by immunoblotting using anti-mDia1 antibody. Quantification of mDia1 in the membrane fraction was performed as described in Materials and Methods, with that of the cells expressing FLAG and GFP as a control ($n=3$). (**C**) Enrichment of mDia1 in the membrane fraction by depletion of Liprin-α1 and Liprin-α3. HeLa cells were transfected with scrambled siRNA or a combination of Liprin-α1 and Liprin-α3 siRNAs. The cells were cultured for 48 hours, and cytosolic and membrane fractions were collected and analyzed by immunoblotting using anti-mDia1 antibody. The amount of mDia1 in the membrane fraction of Liprin-α-depleted cells was compared with that of control scrambled siRNA-treated cells ($n=3$). *$P<0.05$, **$P<0.01$.

cells expressing GFP (Fig. 6B). This Rho-mediated membrane accumulation of mDia1 was suppressed by coexpression of Liprin-α3(1–817) (Fig. 6B). We then examined the effect of Liprin-α depletion on the membrane enrichment of mDia in HeLa cells. HeLa cells were transfected with control siRNA or a combination of siRNAs against Liprin-α1 and Liprin-α3. After 48 hours, the cells were collected and the amount of mDia1 in the membrane was examined. The cells depleted of Liprin-αs showed significant enrichment of mDia1 in the membrane fraction compared with the control cells (Fig. 6C).

The above results together suggest that Liprin-α controls the membrane localization of mDia through its binding. We corroborated this action by using immunofluorescence to examine membrane targeting of the mDia N-terminal fragments containing the DID-DD-CC region (Seth et al., 2006; Brandt et al., 2007; Ramalingam et al., 2010; Gorelik et al., 2011). We expressed GFP–mDia1(136–570) and its A256D or I259D mutant in HeLa cells and examined the localization. When GFP–mDia1(136–570) or the A256D or I259D mutants were expressed alone, they localized to the membrane of the extended edge of cells located at the periphery of the cell cluster (Fig. 7A). The mean percentage of cells showing this localization in the cells expressing these constructs was about 43, 69 and 64%, respectively (Fig. 7B). However, when these fragments were coexpressed with Liprin-α3(1–817), only the membrane localization of GFP–mDia1(136–570) was significantly attenuated (Fig. 7A, right panels), with 29% of cells showing the membrane localization (Fig. 7B). These results support our hypothesis that Liprin-α regulates membrane localization of mDia1 through binding to its DID-DD region.

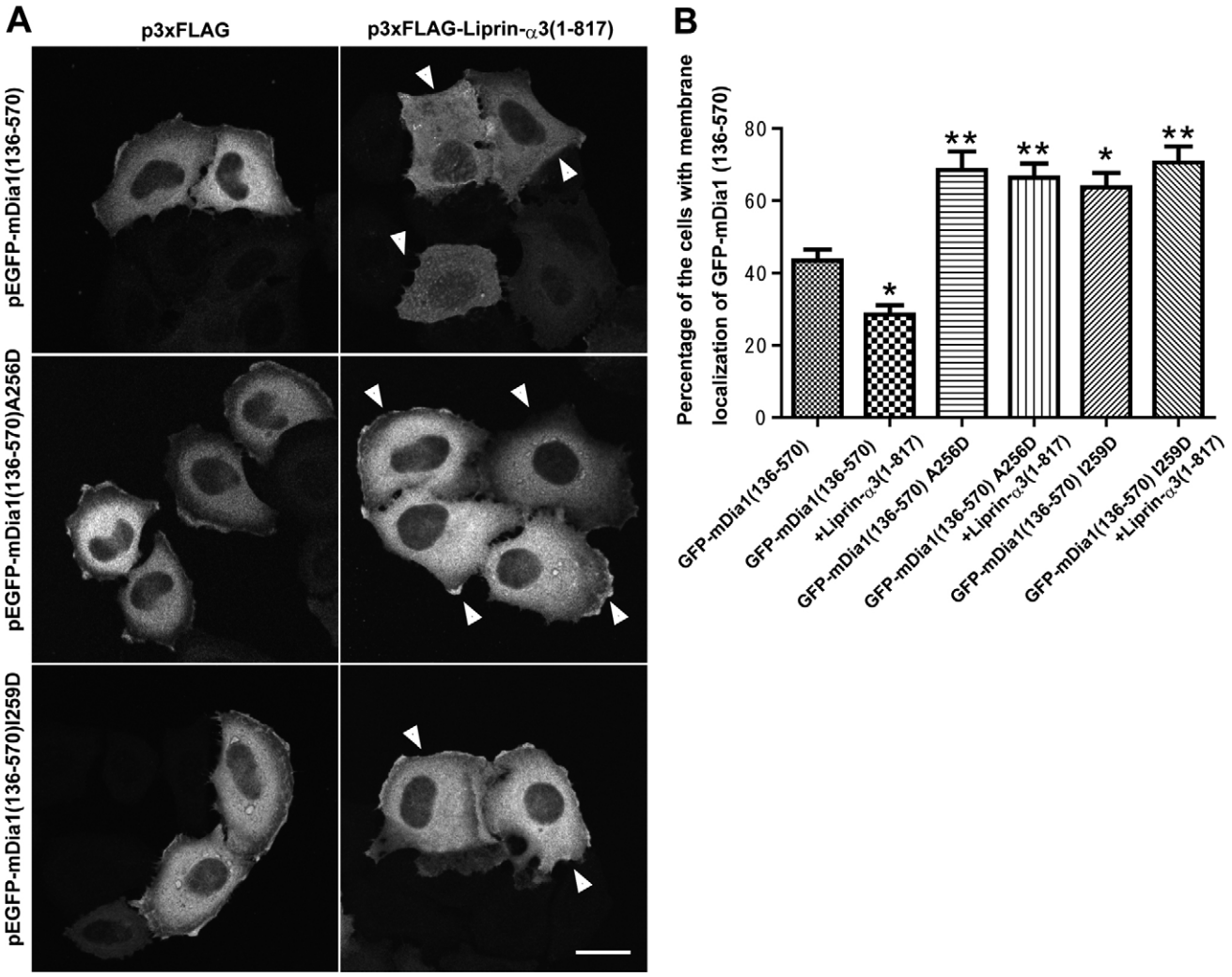

Fig. 7. Membrane localization of GFP–mDia1-DID-DD-CC in HeLa cells and its suppression by overexpression of Liprin-α3 (1–817). (**A**) Immunofluorescence. HeLa cells were transfected with either pEGFP–mDia1(136–570) encompassing the DID-DD-CC region, pEGFP–mDia1(136–570)(A256D) or pEGFP–mDia1(136–570)(I259D) together with p3 × FLAG or p3 × FLAG–Liprin-α3(1–817) and cultured for 18 hours. The cells were fixed with 10% TCA, and stained with anti-GFP and anti-FLAG antibodies. Each image represents a single focal plane of GFP staining. Arrowheads indicate cells expressing FLAG–Liprin-α3(1–817). Scale bar: 20 μm. (**B**) Quantitative analysis of membrane localization of GFP–mDia1(136–570). Experiments were performed as described in A. The percentage of cells showing the membrane localization of the GFP signal in each group was determined by dividing their number by the total number of cells expressing GFP–mDia1(136–570) or mutants. The results are from four independent experiments, in each of which more than 50 cells were examined. *$P<0.05$, **$P<0.01$ compared with cells expressing GFP–mDia1(136–570).

Discussion

In this study, we used GST–mDia1$_N$ as the bait and pulled down Liprin-α3 as an mDia1-binding protein from the mouse brain lysates (Fig. 1B). Immunoprecipitation confirmed interaction of endogenous mDia1 with not only Liprin-α3 but also Liprin-α1 (Fig. 1E,F). Immunoprecipitation analysis (Fig. 2C) demonstrated that all of the three mDia isoforms can bind Liprin-α3. The binding site in mDia1 for Liprin-α3 is localized in its DID-DD domain and apparently overlaps with that for DAD (Fig. 3A,B). Although Liprin-α preferentially binds to an open, active form of mDia (Fig. 3C), it cannot form a ternary complex with mDia and GTP–RhoA (Fig. 3D), indicating that Liprin-α binds to the open form of mDia after GTP–RhoA dissociates from it. Overexpression of the mDia1-binding domain of Liprin-α and RNAi experiments suggest that Liprin-α regulates the amounts of Rho–mDia-mediated actin stress fibers in the cells (Figs 4, 5). Furthermore, biochemical fractionation and immunofluorescence analysis suggest that Liprin-α controls mDia1 localization in the plasma membrane (Figs 6, 7).

A large body of evidence suggests that Diaphanous-related formins (DRFs), including mDia isoforms, stay in the cytosol in an auto-inhibited form through DID-DAD binding and that binding of GTP–Rho to their GBD activates DRFs by disrupting the intramolecular interaction. The DRFs are then recruited to the plasma membrane or other subcellular localization for function through the N-terminal region. Seth and co-workers showed that N-terminal fragments containing GBD, DID and DD regions of mDia and FRLα can localize to the membrane in RAW cells (Seth et al., 2006). They also showed that Rho-binding defective mutants of these fragments still localized to the membrane in a

saturating manner but to a lesser degree, indicating that the membrane localization of mDia1 and FRLα is mediated by both Rho-dependent and Rho-independent interactions and that the latter is through DID binding to unknown partners on the membrane. Brandt and co-workers reported that IQGAP1 binds to the FH3 of mDia1, containing DID-DD-CC regions, and mediates mDia1 localization to the leading edge of migrating cells and the phagocytic cup (Brandt et al., 2007). Recently, Gorelik and colleagues assessed the contribution to membrane targeting of mDia2 of each of the N-terminal basic domains, GBD, DID, DD or CC region and concluded that these regions collectively contribute to plasma membrane localization (Gorelik et al., 2011). These results suggest that binding to the membrane through N-terminal regions is important for the localization and function of mDia proteins, and can be a regulatory step for their function. Our findings that Liprin-α binds to the DID of mDia isoforms, displaces mDia1 from the membrane, and regulates the amount of F-actin in the cell suggest that Liprin-α competes for DID binding with binding protein(s) on the membrane, and induces inactivation of mDia isoforms by membrane dissociation. We propose this as one of the regulatory mechanisms by which mDia controls stress fiber formation in the cell.

Many actin structures produced by formins in the cell (such as stress fibers, actin cables and the contractile ring) are comprised of relatively short actin filaments (0.3–2.3 μm) (Cramer et al., 1997; Kamasaki et al., 2005; Kamasaki et al., 2007). However, purified formins can produce long, often up to 30 μm, actin filaments in vitro (Higashida et al., 2004; Kovar et al., 2006; Paul and Pollard, 2009). It has therefore been questioned how the length of formin-mediated actin filaments is regulated in the cell (Chesarone et al, 2010). Thus far, three formin-binding proteins with inhibitory actions have been identified. They are mammalian Dia-interacting protein (DIP), *Saccharomyces cerevisiae* Bud14 and *Drosophila melanogaster* spire (Chesarone et al., 2009; Eisenmann et al. 2007; Quinlan et al., 2007), all of which inhibit formin-mediated actin polymerization by blocking the FH2 domain. By contrast, Liprin-α targets DID and regulates mDia activity by displacing it from the cell membrane. Such a DID-mediated regulatory mechanism might be consistent with the fact that expression of N-terminally truncated mDia1 mutants lacking DID (such as mDia1ΔN3) induces long actin filaments in the cell (Higashida et al., 2004).

Liprin-α was first identified as an interacting protein of the leukocyte common antigen-related (LAR) family of receptor protein tyrosine phosphatase (Serra-Pages et al., 1995) and suggested to be involved in LAR distribution and clustering (Serra-Pages et al., 1998). Recent studies have shown that depletion of endogenous Liprin-α1 decreases migration and spreading of cultured cells, whereas the overexpression of the protein increased cell migration and spreading (Shen et al., 2007; Asperti et al., 2009). Such action of Liprin-α in cell migration might be consistent with our findings on its role in mDia regulation. Depletion of Liprin-α enhances Rho-mediated formation of focal adhesions (this study), and enhanced Rho activity interferes with cell migration (Raftopoulou and Hall, 2004). Given that mDia1 is also required for cell migration (Yamana et al., 2006), these results suggest that Liprin-α regulates the activity of mDia1 spatiotemporally in the cell to a proper level for migration.

The functions of Liprin-α in neuronal cells have also been reported. In *Drosophila*, both the Liprin-α homolog Dliprin-α and LAR homolog Dlar localize in the presynapse at the neuromuscular junction (NMJ), and both mutants display a decrease in the number of synaptic boutons, an increase in the lengthening of active zones and a reduction in synaptic vesicle release at the NMJ (Kaufmann et al., 2002). Epistasis analysis showed that Dliprin-α is required for the action of Dlar at the synapse, indicating that Dliprin-α and Dlar cooperatively regulate the synaptic growth at the NMJ. Recently, Pawson and co-workers reported that *Drosophila* Diaphanous also localizes in presynapses at NMJ and that Diaphanous mutants showed a decrease in synaptic bouton number at NMJ (Pawson et al., 2008). They also showed that Diaphanous functions downstream of Dlar and the Rho GEF trio, and regulates synaptic growth through the regulation of synaptic actin polymerization and microtubule stabilization. These findings, together with our present study, suggest that Dlar, diaphanous and Dliprin-α might all function in a single signaling pathway, and that Liprin-α might regulate synaptic growth at NMJ by regulating mDia activity and controlling reorganization of the actin cytoskeleton.

In summary, we have identified Liprin-α as a negative regulator of mDia1, and possibly also of other isoforms. Analysis of this function of Liprin-α in other systems might shed a new light on how mDia-mediated actin remodeling is regulated in cell morphogenesis and in shaping of tissue architecture.

Materials and Methods

Materials and constructs

The constructs used in this study are listed in supplementary material Table S1. Proteins used in cell-free experiments were expressed as GST fusions in *Escherichia coli* strain BL21 (DE3) cells (Novagen), and purified as described previously (Watanabe et al., 2010). Primary antibodies used were mouse anti-FLAG M2 monoclonal (Sigma), anti-FLAG polyclonal (Sigma) and mouse anti-vinculin VIN-11-5 monoclonal (Sigma), rabbit anti-GFP polyclonal (MBL), mouse anti-mDia1 Clone 51 monoclonal (BD Transduction Laboratories), rabbit anti-mDia1 polyclonal (used for studies shown in Fig. 6), mouse anti-calnexin monoclonal and chicken anti-Liprin-α1 polyclonal (Abcam), rabbit anti-Liprin-α3 polyclonal (Synaptic Systems), and mouse anti-GAPDH monoclonal (Ambion). Rabbit anti-mDia1 polyclonal antibody used for the study shown in Fig. 1E,F was as previously described (Watanabe et al., 1997). Stealth Select siRNAs for depletion of human mDia1 (#1:HSS102769 and #2:HSS102770) and human and mouse Liprin-α1 and Liprin-α3 were obtained from Invitrogen (supplementary material Table S2).

Isolation and identification of mDia1-binding protein from mouse brain

Mouse whole brain was homogenized in lysis buffer [25 mM Tris-HCl, pH 7.5, 5 mM EDTA and 2 mM β-mercaptoethanol (β-ME)] containing a protease inhibitor mixture (Nacalai Tesque). The homogenate was centrifuged successively at 1000 ***g*** for 15 minutes and at 100,000 ***g*** for 1 hour at 4℃. The 100,000 ***g*** supernatant was incubated with 20 μg of GST–mDia1$_N$, GST–mDia1$_N$ΔG or GST for 1 hour at 4℃, followed by incubation with 30 μl of GSH Sepharose 4 Fast Flow beads (GE Healthcare) for 1 hour at 4℃. After several washings, the beads were boiled in Laemmli buffer (LB). Extracted proteins were run on SDS-PAGE, and either stained with CBB or subjected to immunoblotting using antibodies to Liprin-α1 or Liprin-α3. A 160-kDa protein band detected by CBB staining was excised, digested and subjected to MALDI-TOF mass spectrometric analysis (Shevchenko et al., 1996). All animal experiments were performed according to the relevant regulatory standards.

Analysis of interaction of endogenous proteins

Mouse whole brain was homogenized in RIPA buffer (50 mM Tris-HCl, pH 7.5, 150 mM NaCl, 1% NP40, 1% deoxycholate and 0.1% SDS) containing protease inhibitors with 20 strokes of a Teflon pestle. The homogenate was centrifuged successively at 1000 ***g*** for 10 minutes, and at 100,000 ***g*** for 1 hour at 4℃. The 100,000 ***g*** supernatant was incubated with control non-immune rabbit IgG or anti-mDia1 antibody (Watanabe et al., 1997) together with Protein-G–Sepharose 4 Fast Flow (GE Healthcare) for 2 hours at 4℃. FreeStyle 293F cells were washed once with ice-cold PBS, incubated in lysis buffer (25 mM Tris-HCl, pH 7.5, 150 mM NaCl, 1 mM DTT, 1 mM EDTA and 0.05% Tween20) containing protease inhibitors for 15 minutes at 4℃, sonicated on ice and centrifuged at 12,000 ***g*** for 15 minutes at 4℃. The supernatant was incubated with Protein-G–Sepharose for

30 minutes at 4℃, and centrifuged. Pre-cleared supernatant was then incubated with control non-immune rabbit IgG or anti-mDia1 antibody (Watanabe et al., 1997) together with Protein-G–Sepharose for 2 hours at 4℃. After several washes with lysis buffer, the beads were boiled in 2× LB and extracted proteins were subjected to SDS-PAGE. Immunoblotting was performed using anti-mDia1 (BD Transduction Laboratories), anti-Liprin-α1 and anti-Liprin-α3 antibodies.

Analysis of interaction of expressed proteins

HeLa cells were plated at a density of 1×10^5 cells per 60-mm dish and cultured overnight in Dulbecco's modified Eagle's medium (DMEM) containing 10% FCS. For the experiments shown in Fig. 2B,C and supplementary material Fig. S1C, 3 μg of pEGFP–mDia1$_N$ΔG, pEGFP–mDia2$_N$ΔG, pEGFP–mDia3$_N$ΔG or pEGFP and 1 μg of p3×FLAG plasmids harboring each Liprin-α3 mutant or p3×FLAG were mixed with 5 μl of Lipofectamine LTX (Invitrogen) in 250 μl Opti-MEM (Invitrogen). For the experiments shown in Fig. 3C and supplementary material Fig. S1B, 1 μg of pEGFP–mDia1$_N$ΔG, pEGFP–mDia1(FL), pEGFP–mDia1(FL)(V161D, M1182D) or pEGFP and 3 μg of p3×FLAG–Liprin-α3(FL), p3×FLAG–Liprin-α3(1–817) or p3×FLAG were mixed with 5 μl of Lipofectamine LTX in 250 μl Opti-MEM. The mixture was then added to each 60-mm culture dish. After 18 hours, the cells were washed once with PBS and suspended in 25 mM Tris-HCl, pH 7.4, containing 50 mM NaCl, 1 mM β-ME, 5 mM EDTA and a protease inhibitor cocktail (Roche). The cell suspension was sonicated and centrifuged at 12,000 ***g*** for 15 minutes at 4℃. For the experiments shown in Fig. 2B,C and supplementary material Fig. S1C, the supernatant was incubated with 10 μl of anti-GFP antibody (MBL) and 15 μl of Protein-A–Sepharose (GE Healthcare) for 2 hours at 4℃. For the experiment shown in Fig. 3C and supplementary material Fig. S1B, the supernatant was incubated with 10 μl of anti-FLAG M2 affinity gel (Sigma) for 2 hours at 4℃. Immune complexes were analyzed by immunoblotting using mouse anti-FLAG monoclonal antibody or rabbit anti-GFP polyclonal antibodies.

Analytical gel filtration

mDia1$_N$ and Liprin-α3(457–737) were prepared by cleavage off GST from GST–mDia1$_N$ and GST–Liprin-α3(457–737), respectively, and then incubated in 100 μl of 25 mM Tris-HCl, pH 7.5, containing 150 mM NaCl and 5 mM DTT for 30 minutes at 4℃. Either Liprin-α3(457–737), mDia1 or a mixture of the two, each in 100 μl of the above buffer, was applied to a Sephadex G200 10/30 column (GE Healthcare) equilibrated with the same buffer. Gel filtration was performed at 4℃ with a flow rate of 0.25 ml/minute on the ÄKTA system (GE Healthcare), and each 0.5 ml fraction was collected. Elution of protein was monitored by the absorbance at 280 nm. A 10 μl aliquot of each fraction was boiled in 2× LB, run on SDS-PAGE and analyzed by CBB staining.

Surface plasmon resonance measurement

Protein interaction analysis was performed using BIAcore T100 (GE Healthcare). Purified GST–Liprin-α3(671–737) was captured onto a CM5 sensor chip using a GST kit for fusion capture (GE Healthcare). Subsequent binding experiments were performed in 50 mM Tris-HCl, pH 7.5, containing 300 mM NaCl and 0.005% Tween 20. Multicycle kinetics analysis was performed by regenerating the sensor chip in 10 mM glycine-HCl, pH 2.0. The association (k_a) and dissociation (k_d) rate constants were determined by fitting of the biosensor curves using a BIAcore T100 evaluation software. The equilibrium dissociation constant (K_D) value was calculated from the relation $K_D = k_d/k_a$.

Pull-down experiments

Liprin-α3(457–737) was prepared as above. In the experiment shown in Fig. 3A, 30 μg of either GST–mDia1$_N$ΔG, GST–mDia1$_N$ΔG(A256D), GST–mDia1$_N$ΔG(I259D) or GST were bound to 15 μl of GSH Sepharose, and incubated separately with 120 μg of Liprin-α3(457–737) in 300 μl of 30 mM Tris-HCl, pH 7.5, containing 50 mM NaCl, 5 mM $MgCl_2$, 3 mM β-ME and 0.1% Triton X-100 for 1 hour at 4℃. The beads were spun down and washed three times with the above buffer. In the experiment shown in Fig. 3D, recombinant RhoA was prepared, and GTPγS loading was carried out as described (Watanabe et al., 2010). Ten μg of GDP–RhoA or GTPγS–RhoA was incubated with 10 μg of GST or GST–mDia1$_N$ conjugated to GSH Sepharose in 25 mM Tris-HCl, pH 7.5, containing 5 mM $MgCl_2$, 2 mM EDTA, 100 mM NaCl, 0.05% Tween 20 and 5 mM DTT for 1 hour at 4℃. After several washes with the above buffer, 50 μg of Liprin-α3(457–737) was added and incubated for 1 hour at 4℃. GST or GST–mDia1$_N$ was recovered by centrifugation. Proteins were extracted with LB, subjected to SDS-PAGE and analyzed by CBB staining.

Fluorescence polarization assay

Fluorescence polarization assay using an mDia1 DAD peptide (Rose et al., 2005) was performed as described previously (Watanabe et al., 2010). An mDia1 DAD peptide(1175–1196) labeled with FITC at the N-terminus was synthesized by Invitrogen. After the baseline fluorescence of 50 nM FITC-DAD was obtained, 150 nM mDia1$_N$ was added, and fluorescence was measured with an interval of 10 seconds. At 180 seconds, 450 nM Liprin-α3(457–737) was added, and changes in polarization were recorded.

Fluorescence staining analysis of F-actin and cell morphology

For the overexpression experiments shown in Fig. 4 and supplementary material Fig. S2, 0.5 μg of either pEGFP, pEGFP–V14RhoA, pEGFP–mDia1ΔN3, or pEGFP–mDia1(FL)(V161D, M1182D) and 2 μg of either p3×FLAG or p3×FLAG–Liprin-α3(1–817) were mixed with 3 μl of Lipofectamine LTX in 250 μl Opti-MEM. The mixture was added to HeLa cells that were plated at a density of 5×10^4 cells per 35-mm dish and cultured overnight in DMEM containing 10% FCS. Cells were cultured for 16 hours, washed with PBS, and fixed with 4% formaldehyde in PBS. For the RNAi experiments shown in Fig. 5 and supplementary material Figs S3 and S4, 1 μl of 20 μM siRNA was mixed with 4 μl of Lipofectamine RNAiMAX (Invitrogen) in 200 μl of Opti-MEM. HeLa cells and NIH 3T3 cells of semi-confluency were treated with trypsin–EDTA and suspended, and the siRNA mixture was added to 1.0×10^5 HeLa cells or 5×10^4 NIH 3T3 cells in 1.8 ml of the culture medium. The cells were then seeded on a cover glass, in a well of a six-well plate, and cultured for 48 hours. For quantification of F-actin fluorescence intensity, the cells were trypsinized at 24 hours after siRNA transfection, and mixed with non-transfected cells labeled with DiI (Invitrogen) at a ratio of 9:1, and cultured for 24 hours at 37℃. The cells were washed with PBS, and fixed with 4% formaldehyde in PBS. Permeabilization and incubation with antibodies were performed as described (Ishizaki et al. 2001). Primary antibodies used were anti-FLAG monoclonal (1:200), anti-FLAG polyclonal (1:200) or anti-vinculin monoclonal (1:200). Secondary antibodies included Alexa-Fluor-488-conjugated goat anti-mouse IgG, Alexa Fluor 488 goat anti-rabbit IgG or Alexa Fluor 594 goat anti-rabbit IgG (Molecular Probes). F-actin was stained with Alexa-Fluor-647–phalloidin (1:100; Molecular Probes) or Texas-Red–X-phalloidin (1:100; Molecular Probes). Immunofluorescence images were collected with a LSM510 confocal laser-scanning microscope (Carl Zeiss) using an oil immersion objective lens (Plan-Apochromat 63× 1.4 NA oil DIC), and the 0.5 μm-thick optical section of the bottom was used for analysis. Quantification of F-actin intensity was performed using ImageJ software (http://rsbweb.nih.gov/ij). In brief, each transfected or non-transfected cell in the same field was outlined and the mean phalloidin fluorescence intensity was determined in each cell. The fluorescence intensity of each transfected cell was normalized by dividing the mean phalloidin fluorescence intensity of each cell by the average of those of non-transfected cells (>3) in the same field. We also used ImageJ software to determine the average of focal adhesion areas and the number of focal adhesions per cell in supplementary material Figs S2 and S3. Briefly, each transfected cell was outlined, and thresholded images of vinculin-positive clusters were obtained. Focal adhesion areas larger than 0.1 μm^2 were measured and averaged, and the number of focal adhesions per cell was determined. The ratio of the long axis to the short axis in Fig. 3D was also determined using ImageJ software.

Quantification of membrane localization of mDia1

For the experiments shown in Fig. 6A, HeLa cells were starved in DMEM containing 0.5% FCS for 24 hours and stimulated with 10% FCS at the indicated times. For the experiments shown in Fig. 6B, transfection of plasmid DNA was performed as described above. After 3 hours, the medium was changed to Opti-MEM, and the cells were starved in Opti-MEM for 15 hours. For the experiments shown in Fig. 6C, HeLa cells were transfected with siRNA and cultured in DMEM containing 10% FCS for 48 hours. Cellular fractionation to the cytosol and membrane fractions was performed using a Native Membrane Protein Extraction Kit (M-PEK) according to the manufacturer's protocol (Merck). Each fraction was subjected to SDS-PAGE and immunoblotting was performed. Protein band intensities were measured using Adobe Photoshop. The standard curve for immunoblotting of mDia1 was constructed by applying graded membrane fractions of control cells in each experiment, and the intensity of the sample bands was expressed as the fold change compared with the control band.

Immunofluorescence analysis of membrane localization of mDia1 DID-DD-CC fragments

HeLa cells were transfected with 0.5 μg of either pEGFP–mDia1(136–570), pEGFP–mDia1(136–570)(A256D) or pEGFP–mDia1(136–570)(I259D) together with 2 μg of either p3×FLAG or p3×FLAG–Liprin-α3(1–817) as described above. Cells were fixed at 18 hours after transfection with 10% TCA on ice for 10 minutes. The fixed cells were stained with anti-GFP polyclonal (1:200; MBL) and anti-FLAG monoclonal (1:200) antibodies. Secondary antibodies were Alexa-Fluor-488-conjugated goat anti-rabbit IgG and Alexa Fluor 594 goat anti-mouse IgG (Molecular Probes). Staining was examined with a Leica SP5 confocal imaging system (Plan-Apochromat 40× 1.25 NA). Optical sections of 0.5 μm thickness were obtained from the bottom to the top of the cell, and the section showing membrane localization of the GFP signal in at least a part of the cell was chosen for analysis. The percentage of cells with plasma membrane localization was determined by dividing the number of cells showing plasma membrane localization by the total number of GFP-positive cells.

Statistical analysis

Data are presented as mean ± s.e.m., and were analyzed by one-way factorial ANOVA or unpaired Student's *t*-test. $P<0.05$ was considered statistically significant.

Acknowledgements

We thank Madoka Terao, Hiroaki Mizuno, Aliza Ehrlich, Megan Li, Kimiko Nonomura and Tae Arai for assistance.

Funding

This work was supported in part by Grants-in-Aid for Scientific Research [grant numbers 18002015 and 23229003] from the Ministry of Education, Culture, Sports, Science and Technology of Japan. S.S. was supported by the Global COE program 'The Center of Frontier Medicine'.

Supplementary material available online at
http://jcs.biologists.org/lookup/suppl/doi:10.1242/jcs.087411/-/DC1

References

Asperti, C., Astro, V., Totaro, A., Paris, S. and de Curtis, I. (2009). Liprin-α1 promotes cell spreading on the extracellular matrix by affecting the distribution of activated integrins. *J. Cell Sci.* **122**, 3225-3232.

Brandt, D. T., Marion, S., Griffiths, G., Watanabe, T., Kaibuchi, K. and Grosse, R. (2007). Dia1 and IQGAP1 interact in cell migration and phagocytic cup formation. *J. Cell Biol.* **178**, 193-200.

Chesarone, M., Gould, C. J., Moseley, J. B. and Goode, B. L. (2009). Displacement of formins from growing barbed ends by Bud14 is critical for actin cable architecture and function. *Dev. Cell* **16**, 292-302.

Chesarone, M. A., DuPage, A. G. and Goode, B. L. (2010). Unleashing formins to remodel the actin and microtubule cytoskeletons. *Nat. Rev. Mol. Cell Biol.* **11**, 62-74.

Cramer, L. P., Siebert, M. and Mitchison, T. J. (1997). Identification of novel graded polarity actin filament bundles in locomoting heart fibroblasts: implications for the generation of motile force. *J. Cell Biol.* **136**, 1287-1305.

Eisenmann, K. M., Harris, E. S., Kitchen, S. M., Holman, H. A., Higgs, H. N. and Alberts, A. S. (2007). Dia-interacting protein modulates formin-mediated actin assembly at the cell cortex. *Curr. Biol.* **17**, 579-591.

Gorelik, R., Yang, C., Kameswaran, V., Dominguez, R. and Svitkina, T. (2011). Mechanisms of plasma membrane targeting of formin mDia2 through its amino terminal domains. *Mol. Biol. Cell* **22**, 189-201.

Hall, A. (2005). Rho GTPases and the control of cell behaviour. *Biochem. Soc. Trans.* **33**, 891-895.

Higashida, C., Miyoshi, T., Fujita, A., Oceguera-Yanez, F., Monypenny, J., Andou, Y., Narumiya, S. and Watanabe, N. (2004). Actin polymerization-driven molecular movement of mDia1 in living cells. *Science* **303**, 2007-2010.

Higashida, C., Suetsugu, S., Tsuji, T., Monypenny, J., Narumiya, S. and Watanabe, N. (2008). G-actin regulates rapid induction of actin nucleation by mDia1 to restore cellular actin polymers. *J. Cell Sci.* **121**, 3403-3412.

Higgs, H. N. (2005). Formin proteins: a domain-based approach. *Trends Biochem. Sci.* **30**, 342-353.

Hotulainen, P. and Lappalainen, P. (2006). Stress fibers are generated by two distinct actin assembly mechanisms in motile cells. *J. Cell Biol.* **173**, 383-394.

Ishizaki, T., Naito, M., Fujisawa, K., Maekawa, M., Watanabe, N., Saito, Y. and Narumiya, S. (1997). p160ROCK, a Rho-associated coiled-coil forming protein kinase, works downstream of Rho and induces focal adhesions. *FEBS Lett.* **404**, 118-124.

Ishizaki, T., Morishima, Y., Okamoto, M., Furuyashiki, T., Kato, T. and Narumiya, S. (2001). Coordination of microtubules and the actin cytoskeleton by the Rho effector mDia1. *Nat. Cell Biol.* **3**, 8-14.

Kamasaki, T., Arai, R., Osumi, M. and Mabuchi, I. (2005). Directionality of F-actin cables changes during the fission yeast cell cycle. *Nat. Cell Biol.* **7**, 916-917.

Kamasaki, T., Osumi, M. and Mabuchi, I. (2007). Three-dimensional arrangement of F-actin in the contractile ring of fission yeast. *J. Cell Biol.* **178**, 765-771.

Kaufmann, N., DeProto, J., Ranjan, R., Wan, H. and Van Vactor, D. (2002). Drosophila liprin-α and the receptor phosphatase Dlar control synapse morphogenesis. *Neuron* **34**, 27-38.

Kovar, D. R., Harris, E. S., Mahaffy, R., Higgs, H. N. and Pollard, T. D. (2006). Control of the assembly of ATP- and ADP-actin by formins and profilin. *Cell* **124**, 423-435.

Lammers, M., Rose, R., Scrima, A. and Wittinghofer, A. (2005). The regulation of mDia1 by autoinhibition and its release by Rho*GTP. *EMBO J.* **24**, 4176-4187.

Moseley, J. B., Sagot, I., Manning, A. L., Xu, Y., Eck, M. J., Pellman, D. and Goode, B. L. (2004). A conserved mechanism for Bni1- and mDia1-induced actin assembly and dual regulation of Bni1 by Bud6 and profilin. *Mol. Biol. Cell* **15**, 896-907.

Otomo, T., Otomo, C., Tomchick, D. R., Machius, M. and Rosen, M. K. (2005). Structural basis of Rho GTPase-mediated activation of the formin mDia1. *Mol. Cell* **18**, 273-281.

Paul, A. S. and Pollard, T. D. (2009). Energetic requirements for processive elongation of actin filaments by FH1FH2-formins. *J. Biol. Chem.* **284**, 12533-12540.

Pawson, C., Eaton, B. A. and Davis, G. W. (2008). Formin-dependent synaptic growth: evidence that Dlar signals via Diaphanous to modulate synaptic actin and dynamic pioneer microtubules. *J. Neurosci.* **28**, 11111-11123.

Pruyne, D., Evangelista, M., Yang, C., Bi, E., Zigmond, S., Bretscher, A. and Boone, C. (2002). Role of formins in actin assembly: nucleation and barbed-end association. *Science* **297**, 612-615.

Quinlan, M. E., Hilgert, S., Bedrossian, A., Mullins, R. D. and Kerkhoff, E. (2007). Regulatory interactions between two actin nucleators, Spire and Cappuccino. *J. Cell Biol.* **179**, 117-128.

Raftopoulou, M. and Hall, A. (2004). Cell migration: Rho GTPases lead the way. *Dev. Biol.* **265**, 23-32.

Ramalingam, N., Zhao, H., Breitsprecher, D., Lappalainen, P., Faix, J. and Schleicher, M. (2010). Phospholipids regulate localization and activity of mDia1 formin. *Eur. J. Cell Biol.* **89**, 723-732.

Rose, R., Weyand, M., Lammers, M., Ishizaki, T., Ahmadian, M. R. and Wittinghofer, A. (2005). Structural and mechanistic insights into the interaction between Rho and mammalian Dia. *Nature* **435**, 513-518.

Sagot, I., Rodal, A. A., Moseley, J., Goode, B. L. and Pellman, D. (2002). An actin nucleation mechanism mediated by Bni1 and profilin. *Nat. Cell Biol.* **4**, 626-631.

Schirenbeck, A., Bretschneider, T., Arasada, R., Schleicher, M. and Faix, J. (2005). The Diaphanous-related formin dDia2 is required for the formation and maintenance of filopodia. *Nat. Cell Biol.* **7**, 619-625.

Serra-Pages, C., Kedersha, N. L., Fazikas, L., Medley, Q., Debant, A. and Streuli, M. (1995). The LAR transmembrane protein tyrosine phosphatase and a coiled-coil LAR-interacting protein co-localize at focal adhesions. *EMBO J.* **14**, 2827-2838.

Serra-Pages, C., Medley, Q. G., Tang, M., Hart, A. and Streuli, M. (1998). Liprins, a family of LAR transmembrane protein-tyrosine phosphatase-interacting proteins. *J. Biol. Chem.* **273**, 15611-15620.

Seth, A., Otomo, C. and Rosen, M. K. (2006). Autoinhibition regulates cellular localization and actin assembly activity of the diaphanous-related formins FRLα and mDia1. *J. Cell Biol.* **174**, 701-713.

Shen, J. C., Unoki, M., Ythier, D., Duperray, A., Varticovski, L., Kumamoto, K., Pedeux, R. and Harris, C. C. (2007). Inhibitor of growth 4 suppresses cell spreading and cell migration by interacting with a novel binding partner, liprin α1. *Cancer Res.* **67**, 2552-2558.

Shevchenko, A., Wilm, M., Vorm, O. and Mann, M. (1996). Mass spectrometric sequencing of proteins silver-stained polyacrylamide gels. *Anal. Chem.* **68**, 850-858.

Spangler, S. A. and Hoogenraad, C. C. (2007). Liprin-α proteins: scaffold molecules for synapse maturation. *Biochem. Soc. Trans.* **35**, 1278-1282.

Yamana, N., Arakawa, Y., Nishino, T., Kurokawa, K., Tanji, M., Itoh, R. E., Monypenny, J., Ishizaki, T., Bito, H., Nozaki, K. et al. (2006). The Rho-mDia1 pathway regulates cell polarity and focal adhesion turnover in migrating cells through mobilizing Apc and c-Src. *Mol. Cell. Biol.* **26**, 6844-6858.

Yasuda, S., Oceguera-Yanez, F., Kato, T., Okamoto, M., Yonemura, S., Terada, Y., Ishizaki, T., Ishizaki, T. and Narumiya, S. (2004). Cdc42 and mDia3 regulate microtubule attachment to kinetochores. *Nature* **428**, 767-771.

Watanabe, N. and Higashida, C. (2004). Formins: processive cappers of growing actin filaments. *Exp. Cell Res.* **301**, 16-22.

Watanabe, N., Madaule, P., Reid, T., Ishizaki, T., Watanabe, G., Kakizuka, A., Saito, Y., Nakao, K., Jockusch, B. M. and Narumiya, S. (1997). p140mDia, a mammalian homolog of Drosophila diaphanous, is a target protein for Rho small GTPase and is a ligand for profilin. *EMBO J.* **16**, 3044-3056.

Watanabe, N., Kato, T., Fujita, A., Ishizaki, T. and Narumiya, S. (1999). Cooperation between mDia1 and ROCK in Rho-induced actin reorganization. *Nat. Cell Biol.* **1**, 136-143.

Watanabe, S., Ando, Y., Yasuda, S., Hosoya, H., Watanabe, N., Ishizaki, T. and Narumiya, S. (2008). mDia2 induces the actin scaffold for the contractile ring and stabilizes its position during cytokinesis in NIH 3T3 cells. *Mol. Biol. Cell* **19**, 2328-2338.

Watanabe, S., Okawa, K., Miki, T., Sakamoto, S., Morinaga, T., Segawa, K., Arakawa, T., Kinoshita, M., Ishizaki, T. and Narumiya, S. (2010). Rho and anillin-dependent control of mDia2 localization and function in cytokinesis. *Mol. Biol. Cell* **21**, 3193-3204.

Table S1. Constructs used in this study

Construct / Cloning sites	Primer / sites	Template
pCR-Blunt BamHI-EcoRV	5'-GCAGATCTATGATGTGCGAGGTGATGCCTAC-3' 5'-CGGATATCCTAGCAGGAGTAAGTCCGGACC-3 BglII-EcoRV	Total cDNA
pGEX-4T-1-mDia1$_N$ EcoRI-XhoI	5'-CGGAATTCGACCCCACTGCTCAGTCATTG-3' 5'-CGCTCGAGTTAATCAATCTGCAGGTGTCGGC-3' EcoRI-XhoI	pEGFP-mDia1 (full length)
pGEX-6P-1-mDia1$_N$ΔG BamHI-XhoI	5'-CGAGATCTGGCCATGATGTACATCCAGGAG-3' 5'-GCCTCGAGTTAATCAATCTGCAGGTGTCGGCA-3' BglII-XhoI	pEGFP-mDia1 (full length)
pEGFP-C1-mDia1 (136-570) EcoRI-BamHI	5'- CGGAATTCGGCCATGATGTACATCCAGGAG -3' 5'-CGAGATCTTTAAGCAGCACTGCTAGAAACAGAAG -3' EcoRI-BglII	pEGFP-mDia1 (full length)
pEGFP-C1-mDia1$_N$ΔG EcoRI-BamHI	5'-CGGAATTCGGCCATGATGTACATCCAGGAG-3' 5'-CTAGATCTTTAATCAATCTGCAGGTGTCGGCA-3' EcoRI-BglII	pEGFP-mDia1 (full length)
pEGFP-C1-mDia2$_N$ΔG BglII-EcoRI	5'-CGAGATCTTCACCTCAGGAATTTCTCCATG-3' 5'-GCGAATTCTTAGTCCAAATCTAGTCTTTTTCTGT-3' BglII-EcoRI	pEGFP-mDia2 (full length) (Yasuda et al., 2004)
pEGFP-C1-mDia3$_N$ΔG XhoI-BamHI	5'-CGCTCGAGCTTCTTCACAAGAATATGTTCATGAATT-3' 5'-CGGGATCCTTAGTCTATGCGCTGCCGGTACTT-3' XhoI-BamHI	pEGFP-mDia3 (full length) (Yasuda et al., 2004)
p3xFLAG-Liprin-α3 (FL) HindIII-SmaI	5'-GCAAGCTTATGATGTGCGAGGTGATGCCTAC-3' 5'-CGGATATCCTAGCAGGAGTAAGTCCGGACC-3' HindIII-EcoRV	pCR-Blunt-Liprin-α3 (full length)
p3xFLAG-Liprin-α3 (1-817) HindIII-BglII	5'-GCAAGCTTATGATGTGCGAGGTGATGCCTAC-3' 5'-CGAGATCTTTACCTCCTGTCCTTATCTCCTGG-3' HindIII-BglII	p3xFLAG-Liprin-α3 (full length)

p3xFLAG-Liprin-α3 (817-1194) HindIII-BglII	5’-CGAAGCTTAGGAACAAGAGGAAGCACGAA-3’ 5’-CGAGATCTCTAGCAGGAGTAAGTCCGGAC-3’ HindIII-BglII	p3xFLAG-Liprin-α3 (full length)
p3xFLAG-Liprin-α3 (1-217) HindIII-BglII	5’-GCAAGCTTATGATGTGCGAGGTGATGCCTAC-3’ 5’-CGAGATCTTTAATCCCCATCCTTGCC-3’ HindIII-BglII	p3xFLAG-Liprin-α3 (full length)
p3xFLAG-Liprin-α3 (217-817) HindIII-BglII	5’-CGAAGCTTGATGGACAGACCCTTGCCAAT-3’ 5’-CGAGATCTTTACCTCCTGTCCTTATCTCCTGG-3’ HindIII-BglII	p3xFLAG-Liprin-α3 (full length)
p3xFLAG-Liprin-α3 (417-817) HindIII-BglII	5’-CGAAGCTTCGGCAGAGGGAGAAAATGAAC-3’ 5’-CGAGATCTTTACCTCCTGTCCTTATCTCCTGG-3’ HindIII-BglII	p3xFLAG-Liprin-α3 (full length)
p3xFLAG-Liprin-α3 (617-817) HindIII-BglII	5’-CGAAGCTTATCAAGCTAATTCAAGAAGAGAAA-3’ 5’-CGAGATCTTTACCTCCTGTCCTTATCTCCTGG-3’ HindIII-BglII	p3xFLAG-Liprin-α3 (full length)
pGEX-6P-1-Liprin-α3 (457-737) BamHI-XhoI	5’-CGGAATTCGAGGAGAAGAACTCACTGAGTG-3’ 5’-CGCTCGAGTTATGACCCTGCTTGCAGCGCC-3’ BamHI-XhoI	p3xFLAG-Liprin-α3 (full length)
pGEX-6P-1-Liprin-α3 (671-737) BamHI-XhoI	5’-CGGAATTCAGCTCTGGCCATTCCACCC-3’ 5’-CGCTCGAGTTATGACCCTGCTTGCAGCGCC-3’ BamHI-XhoI	p3xFLAG-Liprin-α3 (full length)

Table S2. siRNAs used in this study

siRNA		Accession number
Human Liprin-α1 (#1)	5'-CCACGAGGAAGACCTTGCTAAAGTA-3'	NM_177423
Human Liprin-α1 (#2)	5'-CCGACCTGGACAAACTGGCAAAGAA-3'	NM_177423
Human Liprin-α3 (#1)	5'-CAGCTCTGACGAAGGAGCTGAACTT -3'	XM_003660
Human Liprin-α3 (#2)	5'-GCCGTCTCTTTGGCAAGAAAGAGAA-3'	XM_003660
Mouse Liprin-α1 (#1)	5'-GAGGCAGCTCAATACTGCACTTCCA-3'	XM_918243
Mouse Liprin-α1 (#2)	5'-CATCTCCCTCTATGCAGCCAAAGAA-3'	XM_918243